Applied Catalysis B: Environmental 199 (2016) 230–240

Contents lists available at ScienceDirect

Applied Catalysis B: Environmental

journal homepage: www.elsevier.com/locate/apcatb

Oxygen vacancy enhanced photostability and activity of plasmon-Ag composites in the visible to near-infrared region for water purification

Huanhuan Ji[a,b], Lai Lyu[a,b], Lili Zhang[a], Xiaoqiang An[a], Chun Hu[a,b,*]

[a] Key Laboratory of Drinking Water Science and Technology, Research Center for Eco-Environmental Sciences, Chinese Academy of Sciences, Beijing 100085, China

[b] University of Chinese Academy of Sciences, Beijing 100049, China

ARTICLE INFO

Article history:
Received 18 March 2016
Received in revised form 9 June 2016
Accepted 13 June 2016
Available online 15 June 2016

Keywords:
Oxygen vacancy
Interfacial charge transfer
Plasmonic-Ag composites
Ag^+ releasing
Entire solar spectrum

ABSTRACT

Solid solution of BiOBr and BHO ($BiO(OH)_{0.06}Br_{0.94}$) with abundant oxygen vacancies was supported on Ag/AgBr using precipitation and deposition–precipitation methods. The photocatalyst showed high and stable photocatalytic activity for the degradation of chlorophenols and azodyes in water under visible to NIR light irradiation without any release of Ag^+, which came from visible-excited AgBr and the SPR of Ag NPs in the visible and NIR region. The different interfacial charge-transfer processes were verified on the basis of cyclic voltammetry analyses and all experimental information. The conduction band (CB) electrons of photoexcited AgBr reacted with the adsorbed oxygen forming $O_2^{\bullet-}$, while the valence band (VB) holes of AgBr were transported the VB of $BiO(OH)_{0.06}Br_{0.94}$ to oxidize organic pollutants or H_2O to $^{\bullet}OH$. The plasmon-induced electrons from Ag NPs transferred to the CB of AgBr reacting with the adsorbed oxygen to $O_2^{\bullet-}$, while the electrons trapped on the oxygen vacancies of $BiO(OH)_{0.06}Br_{0.94}$ transferred to Ag NPs recombining with the plasmon-induced holes, inhibiting the release of Ag^+, and the resulted VB holes of $BiO(OH)_{0.06}Br_{0.94}$ oxidized organic compound. These interfacial charge transfers evidenced the high photoactivity and photostability of $BiO(OH)_{0.06}Br_{0.94}$/Ag/AgBr.

1. Introduction

Photocatalytic solar-energy conversion has been identified as a robust new method for water purification and hydrogen generation at a lower cost and energy consumption [1]. To date, extensive development has been conducted on UV- and visible-light-active photocatalysts, such as UV-active TiO_2 and doped TiO_2 with anions and/or cations [2,3] in the visible range. However, in the entire solar spectrum reaching the earth, 3%, 44%, and 53% are in the UV, visible and near-infrared (NIR) light regions, respectively. Therefore, it is important to develop an efficient photocatalyst in the visible and NIR light regions from the viewpoint of usable solar energy. Unfortunately, only a small number of semiconductors have NIR absorption and activity [4]. A variety of efforts have been undertaken, including converting NIR light (approximately 980 nm) into visible and UV light through the use of up-conversion materials [5] and assembling quantum dot-metal hybrid nanostructures with a designed band structure configuration for NIR-active photocatalysts [6].

An alternative strategy to improve performance is to use the surface-localized plasmon resonance (SPR) energy of irradiated noble metals (Au, Ag, Pt) deposited on semiconductors [7]. By manipulating the composition, shape, and size of plasmonic nanoparticles (NPs), it is possible to use the entire solar spectrum and to extend the absorption band of composite photocatalysts to regions that might be inaccessible to the semiconductors [8,9]. To date, a series of plasmonic photocatalysts [10–14] have been developed for water purification [15,16] and water splitting [17] using visible light. Despite these promising studies, one obstacle to its practical application is the stability of the photoinduced noble metal NPs during photocatalytic reaction. To the best of our knowledge, charge separation at a plasmon-excited metal nanoparticle without corrosion of the particle has never been reported. According to the reported works [7,18], SPR is responsible for the transfer of energetic electrons to adsorbates in the efficient conversion of solar to chemical energy. Moreover, it is worth noting that several findings suggested that energetic holes retained on plasmonic-metal nanoparticles have sufficient energy to drive the oxidation of water and organics on the surface of the metal [19,20]. However, it was observed that the resulting metallic ions were released into

* Corresponding author at: Key Laboratory of Drinking Water Science and Technology, Research Center for Eco-Environmental Sciences, Chinese Academy of Sciences, Beijing 100085, China.
E-mail address: huchun@rcees.ac.cn (C. Hu).

http://dx.doi.org/10.1016/j.apcatb.2016.06.037
0926-3373/

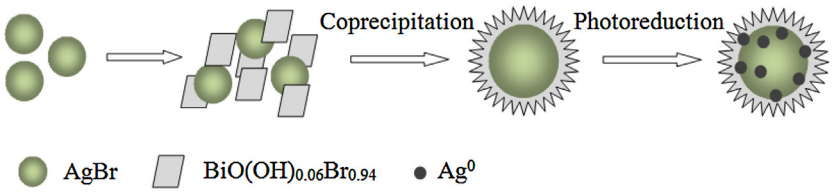

Scheme 1. Synthetic route to the plasmon-Ag composites.

water due to the limited trapping-hole rate from electron donors in solution [21–23]. Therefore, the corrosion and dissolution of the noble metal NPs are inevitable in the photocatalytic reaction, limiting the practical application of plasmonic photocatalysts [24,25].

Interfacial electron and hole transfers with comparable rates have been emphasized as being the most important for maintaining a high photocatalytic efficiency and stability of the noble metal NPs. Surface oxygen vacancies can act as photoinduced charge traps and adsorption sites, in which the charge can transfer to the adsorbed compounds, enhancing the separation of the photogenerated electron-hole pair [26]. Many investigations have indicated that oxygen vacancies play an important role in the process of photocatalysis [27,28]. Moreover, there is higher electron density on the oxygen vacancies, acting as electron donors [29]. It has been determined that adsorbed Au, Ag, and Pt ions on TiO_2 with oxygen vacancies were reduced to form metallic nanoparticles spontaneously [30,31]. Therefore, this reduction can act as an alternative method to control the surface oxygen vacancies for the photostability and activity of plasmon-Ag composites. Either multicomponent oxides with different ion radii and valences or solid solutions with different crystalline phases can be candidates for the surface formation of oxygen vacancies [32]. Bismuth oxyhalide compounds have a layered structure [33], and hydrated bismuth oxide (BHO) is a dihydrate, rather than a trihydrate, also with a layered structure according to previous works [34]. This property makes it feasible for both compounds to form a solid solution.

In the current study, a solid solution of BHO and BiOBr ($BiO(OH)_{0.06}Br_{0.94}$) was prepared by co-precipitation. Moreover, the solid solution-coated Ag/AgBr ($BiO(OH)_{0.06}Br_{0.94}$/Ag/AgBr) was obtained using precipitation and deposition–precipitation methods. For the first time, we demonstrated that $BiO(OH)_{0.06}Br_{0.94}$/Ag/AgBr possessed very high photocatalytic activity and stability in the visible to NIR light region for the degradation of phenolic and azodyes compounds, including 2-chlorophenol (2-CP), 2, 4-dichlorophenol (2, 4-DCP), trichlorophenol (TCP), acid red B (ARB), reactive red K-2BP (K-2BP), cationic red X-GRL (X-GRL), and methyl orange (MO), which are highly toxic and difficult to degrade biologically in aquatic systems. Surprisingly, the photocorrosion and dissolution of Ag NPs were only slightly observed throughout light irradiation without the need of electron donors in solution. Photocatalytic and photostable mechanisms were proposed by surface charge transfer processes over the $BiO(OH)_{0.06}Br_{0.94}$/Ag/AgBr suspension with visible or NIR light irradiation.

2. Experimental

2.1. Chemicals and materials

The reagent 5-*tert*-butoxycarbonyl 5-methyl-1-pyrroline N-oxide (BMPO) used as the spin trapping agent in the electron spin resonance studies (ESR) was purchased from the Bioanalytical Lab (Sarasota, FL). 2-CP, 2,4-DCP, TCP, phenol, ARB, K-2BP, X-GRL, MO and all other chemicals were analytical grade purchased from the Beijing Chemical Company and used without further purification.

2.2. Preparation of catalysts

The catalysts were synthesized through a chemical precipitation method. In a typical process, 0.21 g of $AgNO_3$ in 2.3 mL of NH_4OH (25 wt% NH_3) was added to 200 mL of ultrapure water. Then, 8.66 mL of a 0.2 M KBr solution was added dropwise to the above solution, and subsequently, 0.24 g of $Bi(NO_3)_3{\cdot}5H_2O$ in 10 mL of a 60 vol% acetic solution was added dropwise to the suspension and stirred at room temperature for 12 h. The resulting precipitation was collected and washed several times with water and then photoreduced in 200 mL 10 vol% ethanol solution for 2 h under visible light ($\lambda > 420$ nm) irradiation. Next, the product was centrifuged and washed with water to neutral condition and was dried at 70 °C in air. The synthetic route was illustrated in Scheme 1. By the same procedure, at the given amount of $AgNO_3$ (0.21 g), four samples with different component were prepared when changed the amount of $Bi(NO_3)_3{\cdot}5H_2O$ and KBr (Table S1 in SI). It was found that these samples exhibited almost same photoactivity, however, the catalyst with 0.24 g of $Bi(NO_3)_3{\cdot}5H_2O$ dosage, had more higher activity (Fig. S1 in SI), which is used for all of the subsequent experiments.

As references, by the same method, Ag/AgBr was synthesized without $Bi(NO_3)_3{\cdot}5H_2O$, another sample with 0.24 g of $Bi(NO_3)_3{\cdot}5H_2O$ was also prepared without $AgNO_3$, which was

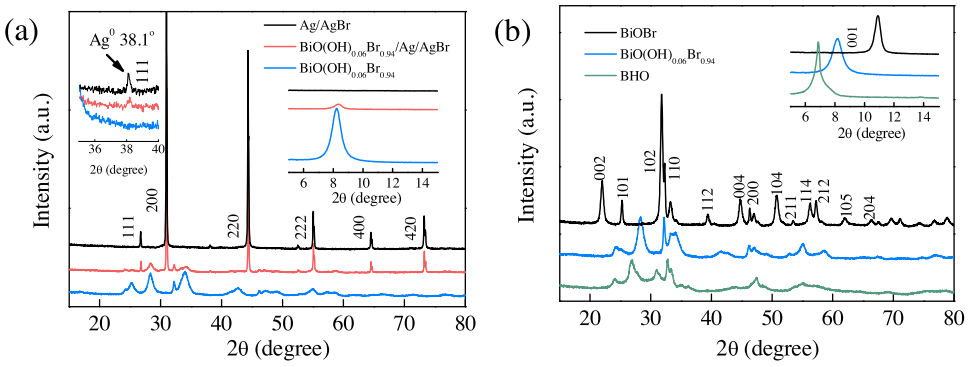

Fig. 1. XRD patterns of different samples (the insets show enlarged figure of 2θ from 36° to 40° of (a) and the low-angle peaks).

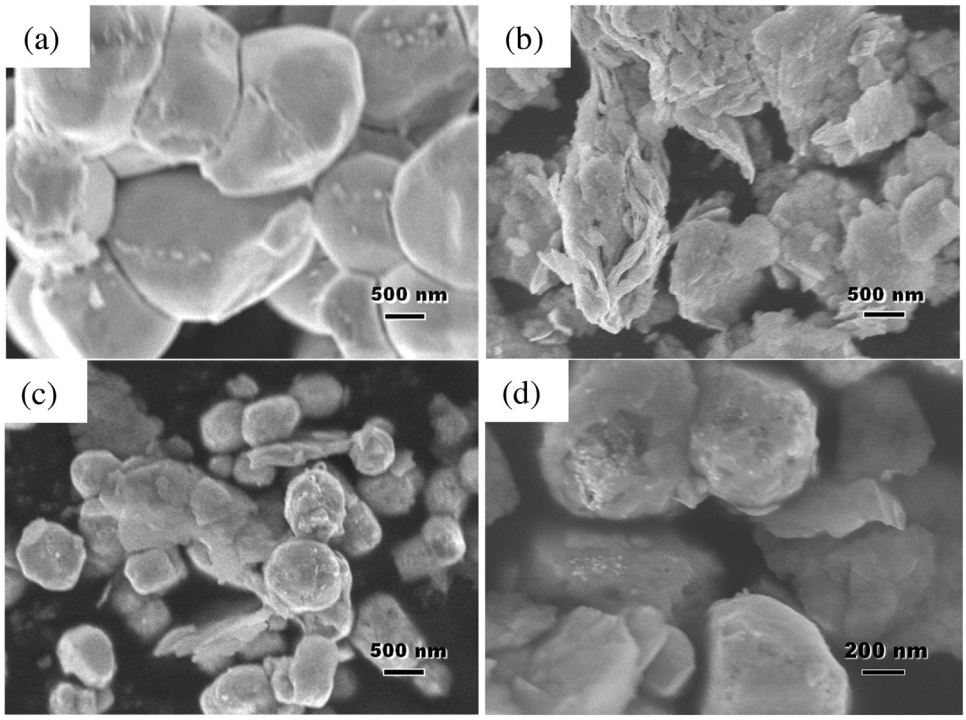

Fig. 2. SEM images of a) Ag/AgBr, b) $BiO(OH)_{0.06}Br_{0.94}$, and c, d) $BiO(OH)_{0.06}Br_{0.94}$/Ag/AgBr.

defined as $BiO(OH)_{0.06}Br_{0.94}$ on the basis of XRD (X-ray diffraction, behind detailed results) and the atomic ratio of Bi and Br determined by ICP-MS (inductively coupled plasma mass spectrometers) and IC (ion chromatography) analysis for the dissolved sample in a H_2SO_4 solution.

BHO sample was prepared by a modified literature method [35]: a solution consisting of 2.3 mL of NH_4OH (25 wt% NH_3) and 200 mL water was prepared, and 0.24 g $Bi(NO_3)_3{\cdot}5H_2O$ dissolved in 10 mL 60 vol% acetic solution was added to the solution. Then, 6 mL NH_4OH was dropwise added to the solution until the white colloid did not formed any longer, subsequently, the colloid was collected and washed, finally, the sampled was dried at 70 °C.

Ag/$BiO(OH)_{0.06}Br_{0.94}$ sample was prepared in dark according to the literature[30]: 0.2 g of the as synthesized $BiO(OH)_{0.06}Br_{0.94}$ was added into 200 mL distilled water under ultrasonication. 0.173 mL of Tollen reagent (0.21 g of $AgNO_3$ in 2.3 mL of NH_4OH) was dropped into the $BiO(OH)_{0.06}Br_{0.94}$ suspension under strong stirring. After 12 h stirring, the final product (denoted as 5% Ag/$BiO(OH)_{0.06}Br_{0.94}$) was collected, washed and dried at 70 °C in an oven.

2.3. Characterization

The samples were characterized by XRD (XDS-2000 diffractometer; Scintag, CA) and UV–vis-NIR diffuse reflectance spectroscopy (Hitachi UH4150). The morphological observations were performed by a field emission scanning electron microscope (SEM) (SU 8020 FESEM; Hitachi). High-resolution transmission electron microscopy (HRTEM) images were recorded using a JEOL-2010 TEM with an acceleration voltage of 200 kV. The X-ray photoelectron spectroscopy (XPS) data were recorded on an AXIS-Ultra instrument using monochromatic Al Kα radiation (225 W, 15 mA, 15 kV) and low-energy electron flooding for charge compensation. To compensate for surface charge effects, the binding energies were calibrated using the C1 s hydrocarbon peak at 284.80 eV. The cyclic voltammetry (CV), photocurrent and Mott-Schottky analysis was measured in a basic electrochemical system (AMETEK Princeton Applied Research, Oak Ridge, TN) with a two-compartment, three-electrode electrochemical cell equipped with a photocatalyst photoanode (prepared by dip-coating and drying in air at 70 °C) and a platinum wire cathode in a 0.1 M Na_2SO_4 solution. The reference electrode was a saturated calomel electrode. The electron-spin resonance (ESR) spectra were obtained using a Bruker model A300-10/12 electron paramagnetic resonance spectrometer. The point of zero charge (pHpzc) of the catalysts was measured with a Zetasizer Nano (Malvern, UK) with three consistent readings.

2.4. Photocatalytic degradation of pollutants under visible to near-infrared light irradiation

Photocatalytic experiments were performed in a beaker with aqueous suspensions of phenolic and azodyes (60 mL, 10 mg L^{-1}) containing 100 mg and 60 mg of catalyst powders, respectively, and the final pH of the aqueous suspensions was adjusted to 9 for chlorophenol degradation. The light source was a 150-W Xe-arc lamp (Shanghai Photoelectron Device Ltd.) equipped with wavelength cutoff filters for $\lambda > 400$, 600 nm, and 800 nm focused onto the beaker. The concentration of each chlorophenol was measured using high-performance liquid chromatography (1200 series; Agilent) with an Eclipse XDB-C18 column (5 μm, 4.6 × 150 mm; Agilent). The concentrations of azodyes were determined with a spectrometer (Hitachi UH3100). The released Ag^+ concentration during photoreaction was determined by an inductively coupled plasma mass spectrometer (ICP-MS, VG Plasma Quad 3). The Cl^- or Br^- concentration in the solution was detected using a Dionex ICS-2000 ion chromatography system with AS-DV autosampler. The total organic carbon (TOC) of each solution was measured with a TOC analyzer (TOC-VCPH, Shimadzu). In the recycling experiments, the photocatalyst was filtered and washed with deionized water prior to being resuspended in the 2-CP or MO solution for another cycle.

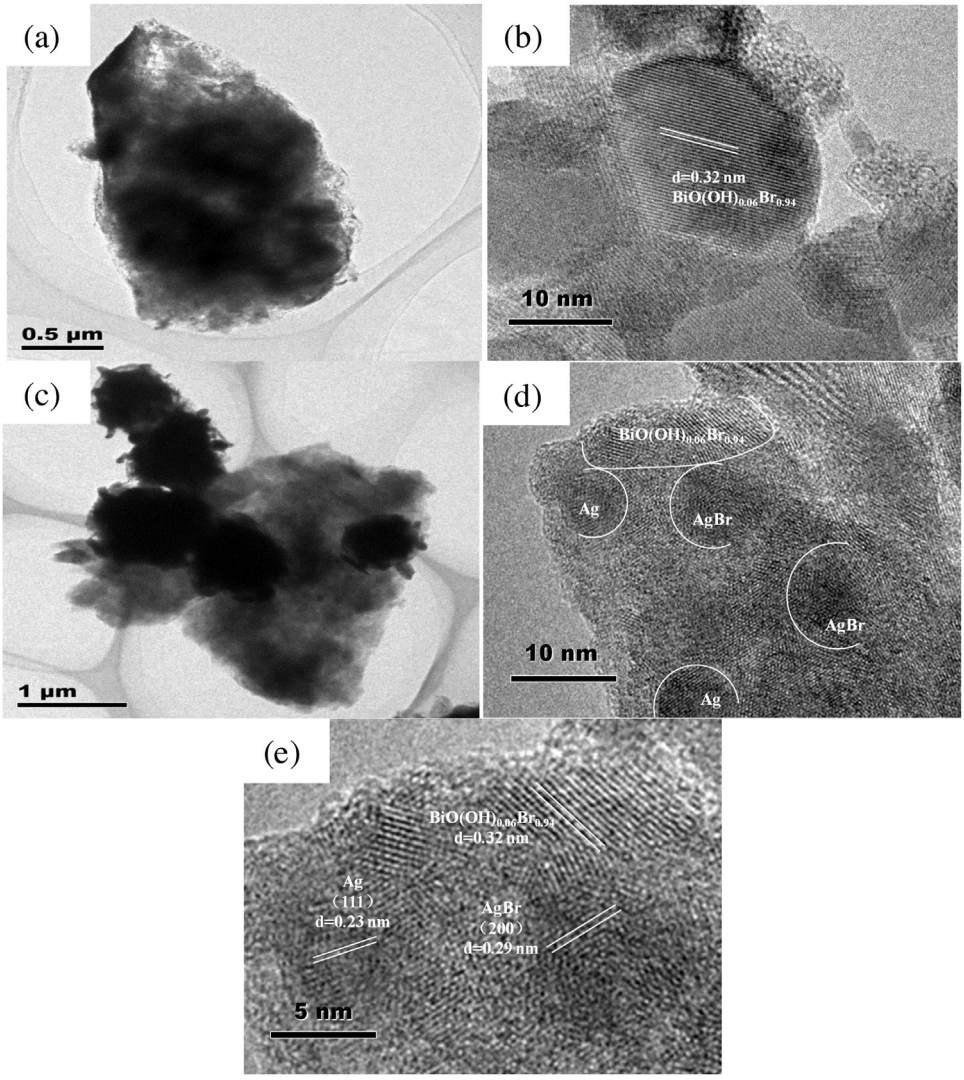

Fig. 3. HRTEM images of a, b) $BiO(OH)_{0.06}Br_{0.94}$ and c, d, e) $BiO(OH)_{0.06}Br_{0.94}$Ag/AgBr.

3. Results and discussion

3.1. Characterization of photocatalysts

Both $BiO(OH)_{0.06}Br_{0.94}$/Ag/AgBr and Ag/AgBr showed the cubic phase of AgBr (JCPDS 06-438), and a weak diffraction peak at 38.0° can be attributed to cubic Ag^0 (JCPDS 65-2871) (Fig. 1a) [36]. The crystallite size of Ag NPs were 34 and 39 nm respectively estimated using the Scherrer equation. In addition, diffraction peaks at 8.3°, 24.3°, 28.4°, 32.2°, and 34.2° were displayed in the sample of $BiO(OH)_{0.06}Br_{0.94}$/Ag/AgBr, which were coincident with the XRD peaks of the as-prepared $BiO(OH)_{0.06}Br_{0.94}$ under identical conditions without the addition of Ag^+. In addition, BiOBr and BHO were prepared under the same conditions without NH_4OH or Br^-, respectively (Fig. 1b) [35]. The XRD peaks of $BiO(OH)_{0.06}Br_{0.94}$ did not match with the peaks of both BiOBr and BHO. However, compared with BiOBr, $BiO(OH)_{0.06}Br_{0.94}$, and BHO, the peak of (001) shifted continuously toward BHO from BiOBr without any impurity phase in $BiO(OH)_{0.06}Br_{0.94}$, indicating that $BiO(OH)_{0.06}Br_{0.94}$ was a solid solution of BiOBr and BHO. The SEM images of Ag/AgBr (Fig. 2a) showed the crystalline sizes were in the range 1–3 μm. The $BiO(OH)_{0.06}Br_{0.94}$ solid solution was a layered structure with micrometer-sized sheets (Fig. 2b). However, the size of the $BiO(OH)_{0.06}Br_{0.94}$/Ag/AgBr particles was below 1 μm. Ag/AgBr was uniformly and compactly coated with $BiO(OH)_{0.06}Br_{0.94}$, and almost all of the Ag NPs were sandwiched between $BiO(OH)_{0.06}Br_{0.94}$ and AgBr (Fig. 2c, d). The results indicated that the coating of $BiO(OH)_{0.06}Br_{0.94}$ inhibited the growth of AgBr and Ag particles. The HRTEM images of $BiO(OH)_{0.06}Br_{0.94}$ exhibited stacked sheets, and showed a lattice spacing of 0.32 nm, indicating the formation of a solid solution (Fig. 3a, b). In Fig. 3c, $BiO(OH)_{0.06}Br_{0.94}$/Ag/AgBr exhibited that the sphere particles were embedded into the sheet, confirming that Ag/AgBr was covered by $BiO(OH)_{0.06}Br_{0.94}$. Three lattice fringe spacings at 0.32 nm, 0.22 nm, and 0.29 nm were observed in the HRTEM image of $BiO(OH)_{0.06}Br_{0.94}$/Ag/AgBr, corresponding to the characteristic lattice fringe of $BiO(OH)_{0.06}Br_{0.94}$, the (111) plane of Ag, and the (200) plane of AgBr (Fig. 3d, e). The element of Bi, O, Br were found in the XPS survey spectrum of $BiO(OH)_{0.06}Br_{0.94}$, and Bi, O, Br, Ag were observed in $BiO(OH)_{0.06}Br_{0.94}$/Ag/AgBr sample (Fig. S2 in SI). On the basis of XPS and AES measurements (Fig. 4a, b), the surface Ag species mainly existed as Ag^+ in $BiO(OH)_{0.06}Br_{0.94}$/Ag/AgBr. In $BiO(OH)_{0.06}Br_{0.94}$, both Br $3d_{5/2}$ and Br $3d_{3/2}$ peaks at 68.6 and 69.6 eV appeared, while in $BiO(OH)_{0.06}Br_{0.94}$/Ag/AgBr, additional Br $3d_{5/2}$ and Br $3d_{3/2}$ peaks at 68.9 and 69.8 eV were observed, which were ascribed to AgBr (Fig. 4c) [37]. The concentration of Bi in the surface of the catalyst was 53.02 wt% according to the XPS data, which was much more than the bulk concentration of

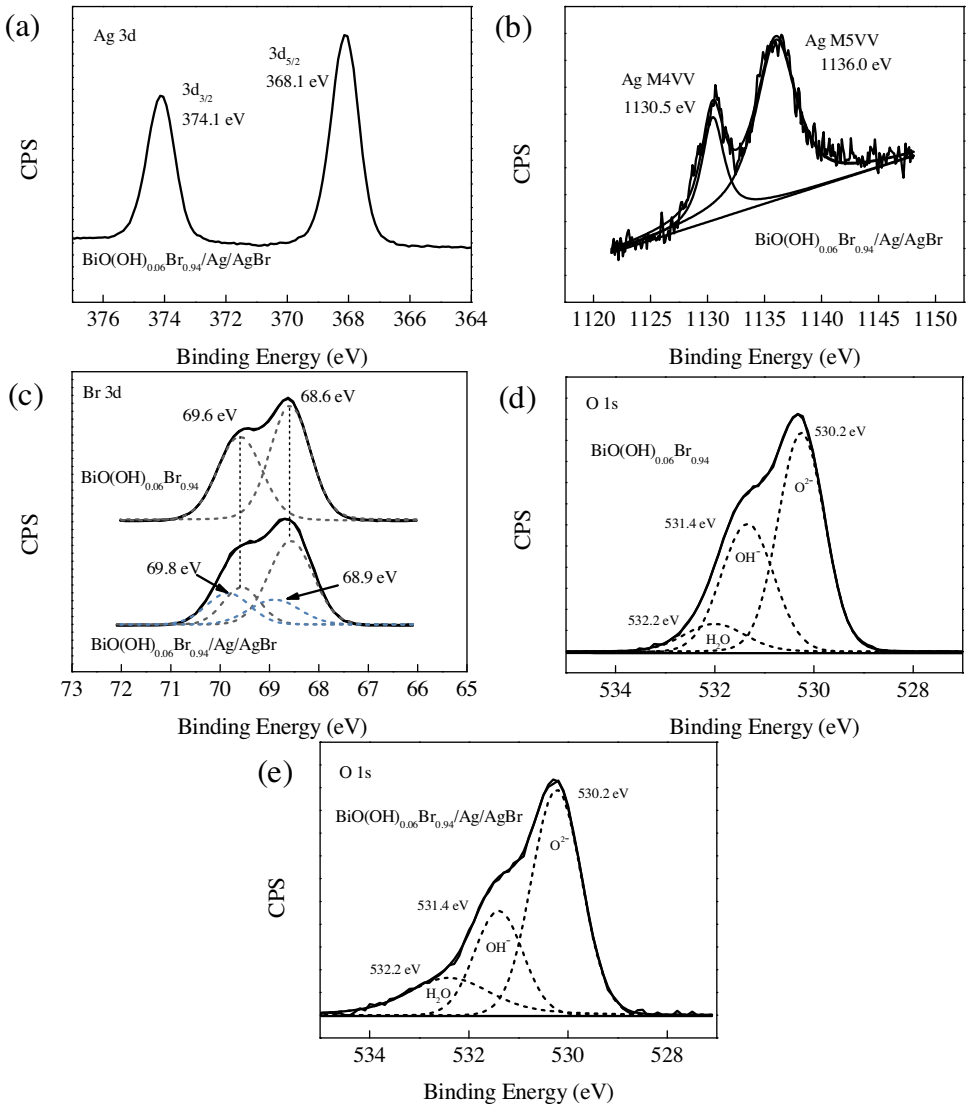

Fig. 4. a) Ag 3d, b) Ag MVV, c) Br 3d, and d, e) O 1 s XPS spectra of the $BiO(OH)_{0.06}Br_{0.94}$/Ag/AgBr and $BiO(OH)_{0.06}Br_{0.94}$ samples.

Bi (25.81%). These results indicated that most of $BiO(OH)_{0.06}Br_{0.94}$ existed on the surface of the composite, while Ag NPs was supported on AgBr. The characterized results indicated that the heterojunctional structure was formed with a good interfacial contact in $BiO(OH)_{0.06}Br_{0.94}$/Ag/AgBr, which is beneficial to interfacial charge carrier transfer. The O 1 s XPS spectra of $BiO(OH)_{0.06}Br_{0.94}$ and $BiO(OH)_{0.06}Br_{0.94}$/Ag/AgBr exhibited three peaks at 530.2 eV, 531.4 eV (Fig. 4d, e), corresponding to the crystal lattice oxygen for O^{2-}, OH^-, while the peak at approximately 532.2 eV is attributed to the defect sites with a low oxygen coordination, i.e. oxygen vacancies [38,39]. The oxygen vacancies were about 2 atom% on the surface of $BiO(OH)_{0.06}Br_{0.94}$/Ag/AgBr by deconvolution of the O 1 s spectra and XPS data. Fig. 5 shows the UV–vis-NIR diffuse reflectance spectra (DRS) of the samples. Both Ag/AgBr and $BiO(OH)_{0.06}Br_{0.94}$/Ag/AgBr exhibited strong absorptions from the UV to the NIR region, while $BiO(OH)_{0.06}Br_{0.94}$ exhibited absorption at wavelengths below the 400 nm region. It is well known that AgBr has a direct band at approximately 290 nm and an indirect band gap at approximately 470 nm [40,41]. The results indicated that the SPR of Ag NPs contributed to the strong absorption of Ag/AgBr and $BiO(OH)_{0.06}Br_{0.94}$/Ag/AgBr in the visible and NIR region.

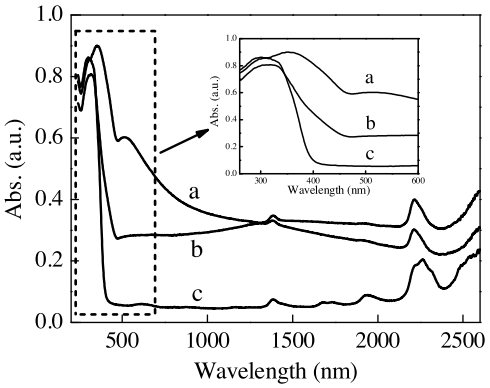

Fig. 5. UV–vis-NIR DRS of different samples: a) Ag/AgBr, b) $BiO(OH)_{0.06}Br_{0.94}$/Ag/AgBr and c) $BiO(OH)_{0.06}Br_{0.94}$.

3.2. Photocatalytic performance under visible to infrared light irradiation

To evaluate the plasmon-induced photocatalytic activity and stability of Ag NPs on Ag/AgBr and $BiO(OH)_{0.06}Br_{0.94}$/Ag/AgBr,

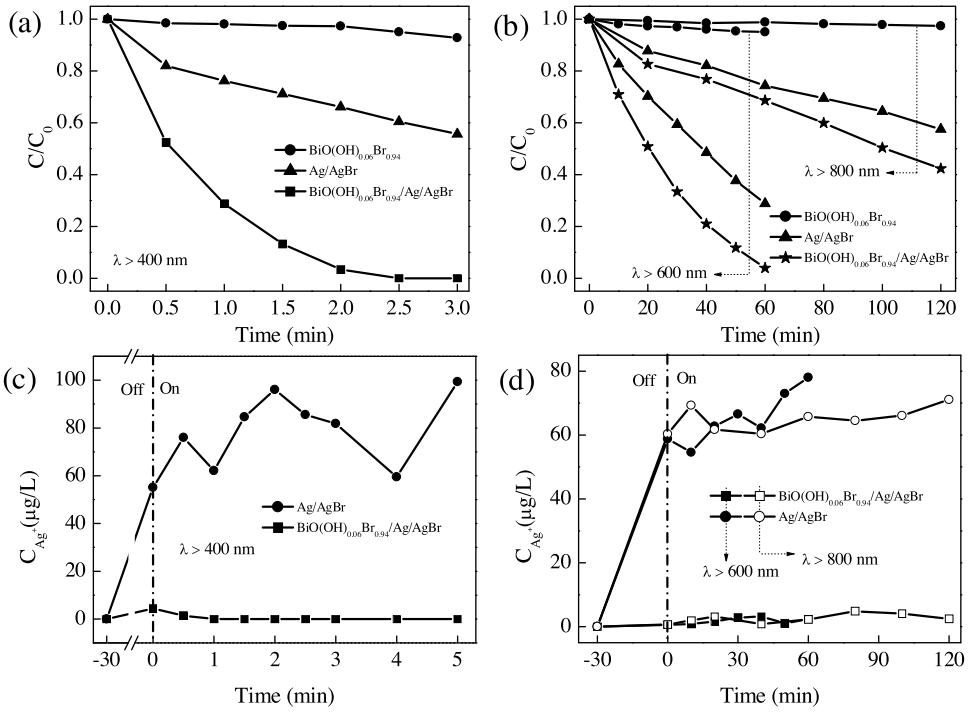

Fig. 6. a, b) 2-CP (10 mg/L, 60 mL) degradation and c, d) the corresponding Ag^+ releasing in aqueous dispersions containing the prepared samples (1.6 g/L) with different light irradiation.

the photodegradation of 2-CP was carried out in aqueous dispersions under different visible and NIR light irradiation at pH 9 after the adsorption equilibrium of 2-CP in the dark (Fig. 6a, b). As comparison, 2-CP degradations were also performed in $BiO(OH)_{0.06}Br_{0.94}$ suspensions under identical conditions. The adsorbed 2-CP were 5.7%, 3.8% and 9.5% on the surfaces of $BiO(OH)_{0.06}Br_{0.94}$/Ag/AgBr, Ag/AgBr, $BiO(OH)_{0.06}Br_{0.94}$, respectively. An almost complete photodegradation of 2-CP was observed at 2.5 min in the $BiO(OH)_{0.06}Br_{0.94}$/Ag/AgBr suspension under visible light irradiation (λ > 400 nm); at the same time, approximately 40% of 2-CP were removed in the Ag/AgBr suspension. Similarly, $BiO(OH)_{0.06}Br_{0.94}$/Ag/AgBr still exhibited the highest activity at wavelengths λ > 600 nm and λ > 800 nm, about 97% and 58% of 2-CP were degraded within 60 min and 120 min. 2-CP was also greatly degraded in the Ag/AgBr suspension with the same irradiation. However, $BiO(OH)_{0.06}Br_{0.94}$ did not show significant activity in the visible to NIR region due to no absorption of light. Because AgBr absorbed slightly in the λ > 600 nm region, the enhanced degradation of 2-CP was due to the SPR of Ag NPs in the materials. During the whole process, Ag^+ ions were hardly released in the $BiO(OH)_{0.06}Br_{0.94}$/Ag/AgBr suspension. In contrast, in the Ag/AgBr suspension, the released Ag^+ concentration was approximately 60 μg/L in the dark, which increased to approximately 99 and 66 μg/L under visible and NIR irradiation, respectively (Fig. 6c, d). The results indicated that Ag NPs were photostable in $BiO(OH)_{0.06}Br_{0.94}$/Ag/AgBr, while it was photocorroded in Ag/AgBr.

In addition, TCP and 2, 4-DCP were almost completely degraded within 1 and 1.5 min, respectively, and approximately 80% of phenol was removed at 10 min in the $BiO(OH)_{0.06}Br_{0.94}$/Ag/AgBr suspension (Fig. 7a). Almost all of the chlorine in 2-CP, 2, 4-DCP, and TCP was converted into Cl^- ions (Fig. 7b), as indicated by the adsorption of Cl^- (2.9 mg saturation adsorption under the identical condition) onto the surface of the catalyst. Moreover, 70%, 70%, 60%, and 50% of TOC were removed after 30 min for 2-CP, phenol, 2, 4-DCP, and TCP, respectively (Fig. 7c). In addition, nonbiodegradable azodyes, i.e., MO, ARB, K-2BP, and X-GRL, were decolorized more than 90% at 10 min in the $BiO(OH)_{0.06}Br_{0.94}$/Ag/AgBr suspension with visible-light irradiation (λ > 400 nm) (Fig. 7d). Furthermore, the catalyst durability was examined for the degradation of 2-CP and MO under visible light, which indicated that the photocatalytic activity did not decrease significantly after ten successive cycles under visible irradiation (Fig. 8a, b). Meanwhile, the catalyst still maintained stable photoactivity for five cycles under NIR irradiation (Fig. 8c). The XRD patterns before and after recycling experiments were almost identical (Fig. 9), confirming the photostability of $BiO(OH)_{0.06}Br_{0.94}$/Ag/AgBr. In contrast, the decolorization percentage of MO decreased from 80% at the first cycle to 47% at the tenth cycle in the Ag/AgBr suspension, indicating its photo-instability (Fig. 8d). The activity and stability of Ag NPs were greatly enhanced in the heterojunctional structures under solar light; $BiO(OH)_{0.06}Br_{0.94}$/Ag/AgBr was confirmed to act as an effective and stable plasmonic photocatalyst.

3.3. Photocatalytic and photostable mechanism of plasmon-Ag composites

Fig. 10 shows the CV data in the dark and under the light (λ > 400 and 800 nm) irradiation obtained from Ag/AgBr and $BiO(OH)_{0.06}Br_{0.94}$/Ag/AgBr electrodes. The oxidation peak of Ag NPs was observed in both dark and light for Ag/AgBr, and its intensities increased after visible and NIR light irradiation, indicating that the plasmon-induced e^- of Ag NPs transferred to the CB of AgBr leading Ag^+ formation (Fig. 10a, b). However, the same phenomena did not occur on the surfaces of $BiO(OH)_{0.06}Br_{0.94}$/Ag/AgBr under identical conditions (Fig. 10c, d). Fig. 11 shows the UV–vis DRS of Ag/$BiO(OH)_{0.06}Br_{0.94}$ prepared in dark without any reducing agent with $AgNO_3$ aqueous solution. The relative UV–vis absorption spectra were obtained by the difference spectra between those of Ag/$BiO(OH)_{0.06}Br_{0.94}$ and $BiO(OH)_{0.06}Br_{0.94}$, which exhibited a SPR absorption band of Ag NPs according to the reported work [7], confirming that the Ag NPs directly growed on the surface of $BiO(OH)_{0.06}Br_{0.94}$, indicating that the Ag^+ could be spontaneously reduced by the electron trapped on the oxygen vacancies of $BiO(OH)_{0.06}Br_{0.94}$. The same phenomena has been observed for

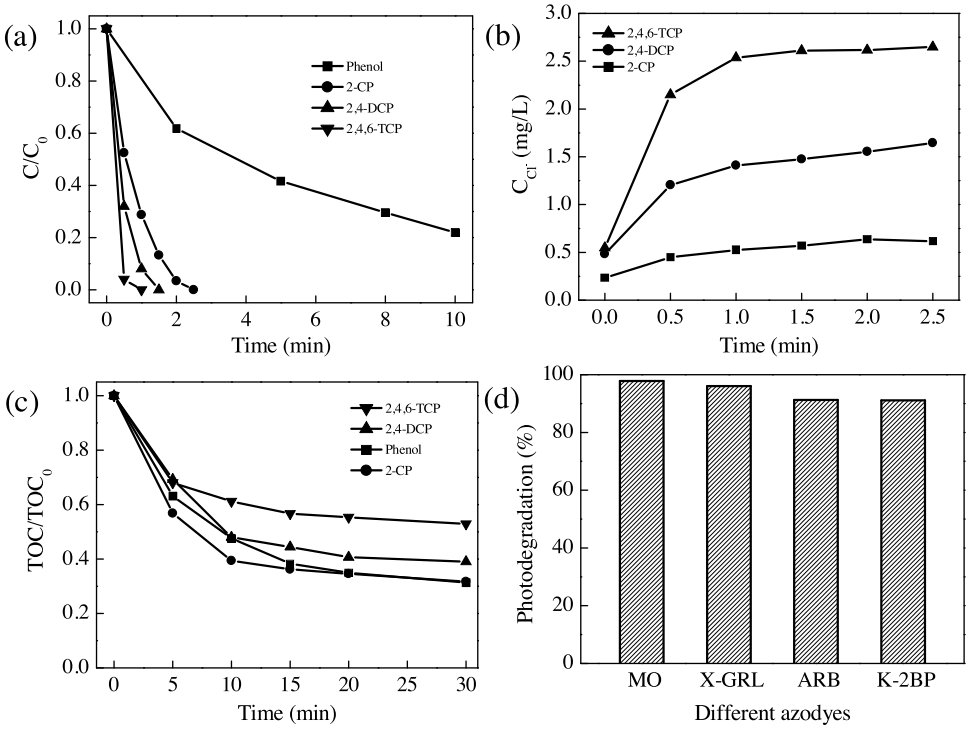

Fig. 7. The temporal course of a) photodegradation, b) dechlorination and c) mineralization of phenolic compounds (10 mg/L, 60 mL) in $BiO(OH)_{0.06}Br_{0.94}$/Ag/AgBr (1.6 g/L) aqueous dispersions and d) photodecoloration of different azodyes (10 mg/L, 60 mL) in $BiO(OH)_{0.06}Br_{0.94}$/Ag/AgBr (1.0 g/L) aqueous dispersions within 10 min under visible light (λ > 400 nm) irradiation.

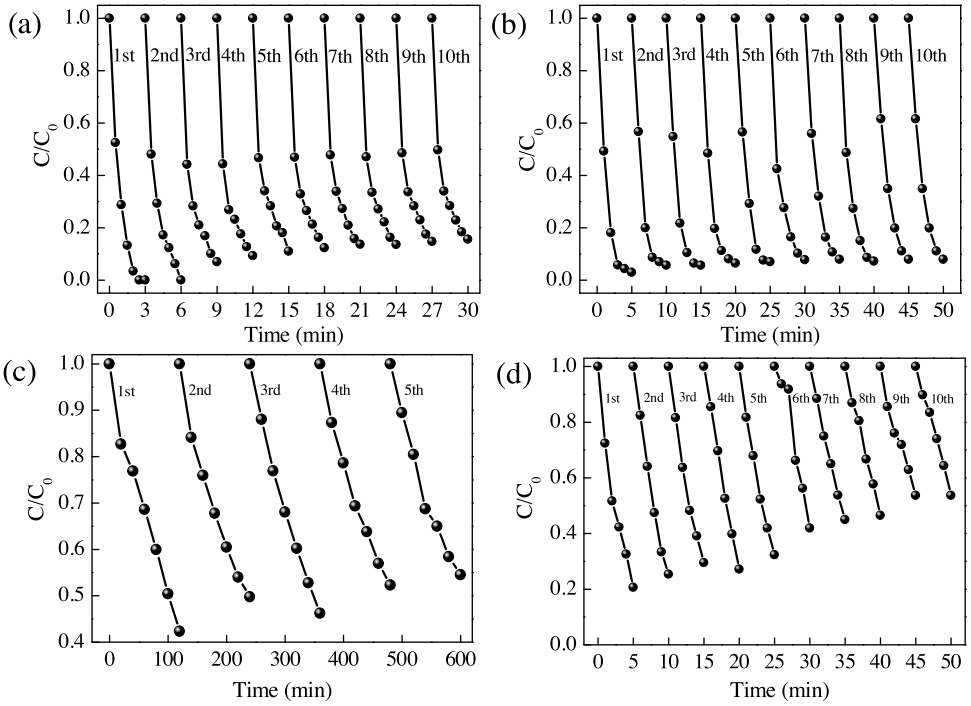

Fig. 8. Cycling runs in the photodegradation of a) 2-CP and b) MO with visible light (λ > 400 nm), or c) 2-CP under near infrared light (λ > 800 nm) irradiation in $BiO(OH)_{0.06}Br_{0.94}$/Ag/AgBr aqueous suspension. And d) cycling runs in the photodegradation of MO in the Ag/AgBr suspension with λ > 400 nm.

the growth of noble metals on the defective TiO_2 with oxygen vancancies [30,31]. Therefore, the photogenerated Ag^+ also could be reduced on the oxygen vacancies of $BiO(OH)_{0.06}Br_{0.94}$, resulting in invisible oxidation peak of Ag NPs on $BiO(OH)_{0.06}Br_{0.94}$/Ag/AgBr under visible and NIR irradiation, although $BiO(OH)_{0.06}Br_{0.94}$ could not be photoexcited under the conditions. The transfer processes of charge carrier were further illustrated by the band structures. The Mott-Schottky plot of the $BiO(OH)_{0.06}Br_{0.94}$ solid solution showed a positive slope, which is typical for a n-type semiconductor (Fig. 12a). The flat band potential of $BiO(OH)_{0.06}Br_{0.94}$ was −0.507 eV vs SCE; thus, the CB edge potential (E_{CB} vs SHE) of $BiO(OH)_{0.06}Br_{0.94}$ was −0.325 eV. The band gap energy (E_g) of

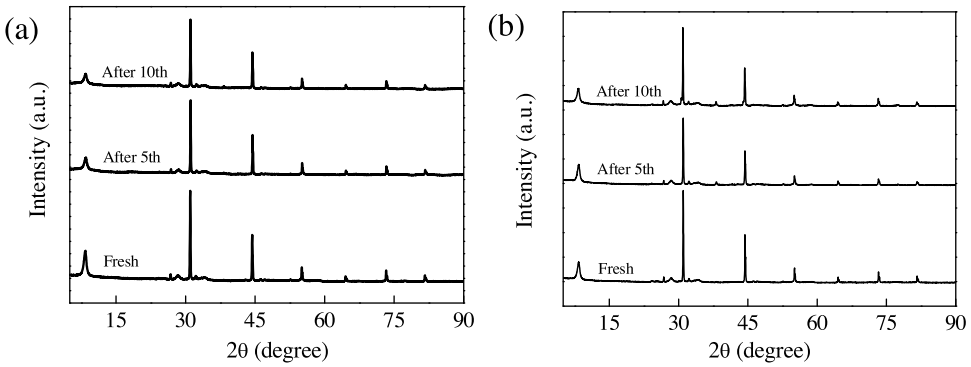

Fig. 9. XRD patterns of $BiO(OH)_{0.06}Br_{0.94}$/Ag/AgBr before and after cycling runs in the photodegradation of (a) 2-CP and (b) MO.

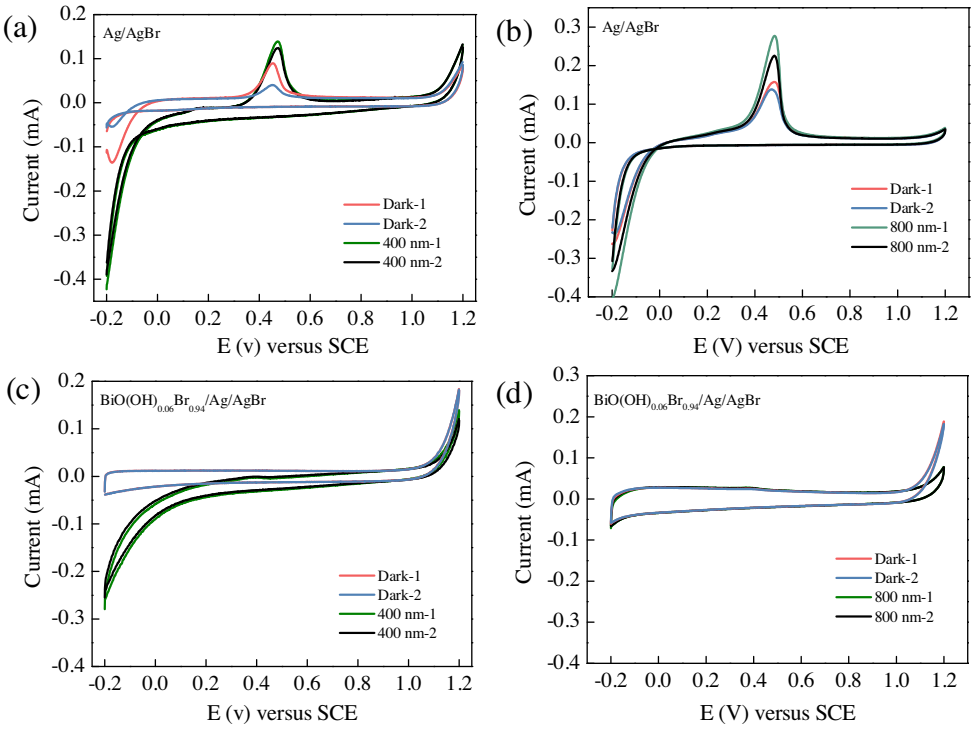

Fig. 10. Cyclic voltammetry of a, b) Ag/AgBr, c, d) $BiO(OH)_{0.06}Br_{0.94}$/Ag/AgBr electrodes under the specified conditions.

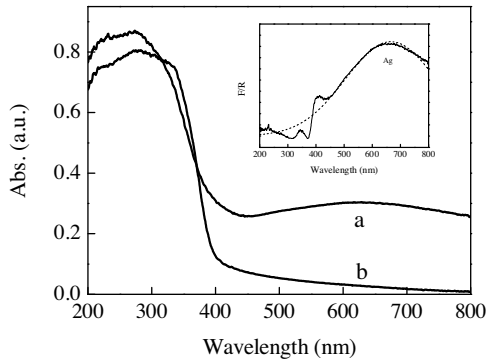

Fig. 11. The UV–vis DRS of a) Ag/$BiO(OH)_{0.06}Br_{0.94}$ and b) $BiO(OH)_{0.06}Br_{0.94}$ sample (the inset shows deconvoluted subbands of 5% Ag/$BiO(OH)_{0.06}Br_{0.94}$).

$BiO(OH)_{0.06}Br_{0.94}$ was 2.937 eV calculated by the absorption edge in the UV–vis DRS spectrum (Fig. 12b); thus, the VB edge potential (E_{VB}) was 2.612 eV vs SHE by $E_{VB} = E_{CB} + E_g$. On the other hand, the work function of Ag NPs is approximately 4.30 eV [42], so its E_{fAg} is −0.24 eV vs SHE. Since energy levels of oxygen vancancies should be below the conducttion band of $BiO(OH)_{0.06}Br_{0.94}$, and it was more negative than the E_{fAg} of Ag NPs according to the reduction of Ag^+ to Ag NPs by e^- existing on the oxygen vacancies [31]. At the interface of Ag/$BiO(OH)_{0.06}Br_{0.94}$, the electron trapped on the oxygen vancancies transfer to Ag NPs, inhibiting the photocorrosion of Ag NPs. According to an empirical equation: $E_{CB} = \chi - E_c - 0.5\ E_g$, where χ is the electronegativity of the semiconductor which is the geometric mean of the electronegativity of the constituent atoms, and E_c is the energy of free electrons on the hydrogen scale (ca. 4.50 eV). E_g and χ of AgBr are 2.69 eV and 5.78 eV; thus, E_{CB} and E_{VB} of AgBr are −0.065 eV and 2.625 eV vs SHE [11]. At the interface of Ag/AgBr, the plasmon-induced electron transfer occurred from Ag NPs to the CB of AgBr, leading to the oxidation of Ag NPs. Similarly, at the interface of $BiO(OH)_{0.06}Br_{0.94}$/AgBr, under visible/NIR irradiation the photogenerated holes of the VB of AgBr would be immigrated to the less positive VB of $BiO(OH)_{0.06}Br_{0.94}$. The transient surface photocurrents of $BiO(OH)_{0.06}Br_{0.94}$/Ag/AgBr were much greater than that one of Ag/AgBr, indicating that the greater separation and migration of photogenerated electron–hole

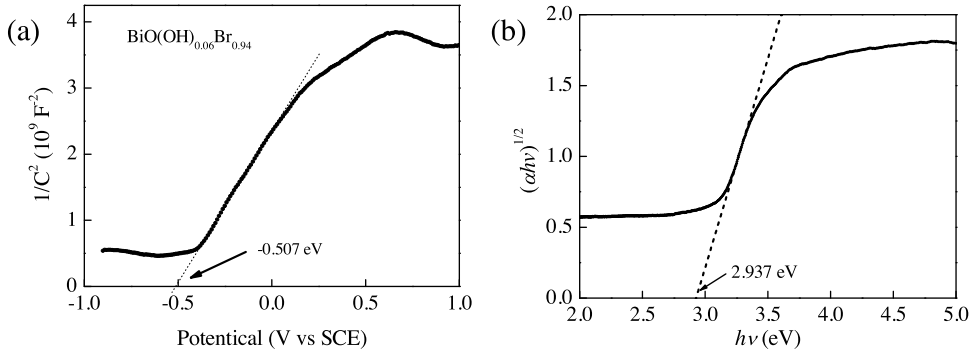

Fig. 12. a) Mott-Schottky diagram of a $BiO(OH)_{0.06}Br_{0.94}$ electrode, b) plots of $(\alpha h\nu)^{1/2}$ versus photon energy ($h\nu$) for the $BiO(OH)_{0.06}Br_{0.94}$ photocatalyst.

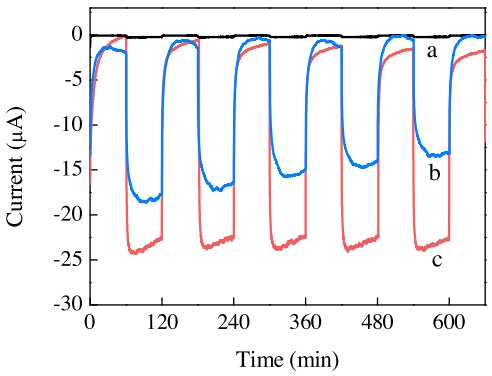

Fig. 13. The transient photocurrent response of different electrodes under visible light (λ > 400 nm) irradiation: a) $BiO(OH)_{0.06}Br_{0.94}$, b) Ag/AgBr and c) $BiO(OH)_{0.06}Br_{0.94}$/Ag/AgBr.

pairs occurred in $BiO(OH)_{0.06}Br_{0.94}$Ag/AgBr (Fig. 13). Correspondingly, the transfer processes were also followed by the ESR spin-trap technique (with BMPO, Fig. 14a, b). The much stronger peaks of BMPO-$O_2^{\bullet-}$ and BMPO-•OH appeared in visible light-irradiation $BiO(OH)_{0.06}Br_{0.94}$/Ag/AgBr suspension. The results verified that the transported holes on the VB of $BiO(OH)_{0.06}Br_{0.94}$ could oxidize the adsorbed H_2O molecule to •OH, while the electrons on the CB of AgBr from photoexcited AgBr and plasmon-induced Ag NPs, could react with adsorbed oxygen producing $O_2^{\bullet-}$. Under NIR irradiation, the much stronger peaks of BMPO-$O_2^{\bullet-}$still was detected in $BiO(OH)_{0.06}Br_{0.94}$/Ag/AgBr suspension than Ag/AgBr suspension, while the •OH radicals were not detected in the same system (Fig. 14c).

The effects of various radical scavengers on the degradation of 2-CP were examined. At λ > 400 nm, the degradation of 2-CP was almost completely depressed by the hole scavenger, triethanolamine (TEOA), and the $O_2^{\bullet-}$ scavenger, *p*-benzoquinone, respectively, while it was depressed to some extent with the addition of the •OH scavenger, *t*-butanol, and the electron scavenger, $K_2S_2O_8$ (Fig. 15a). In particular, the degradation rate of 2-CP was hardly changed at N_2 atmosphere compared with that at an air atmosphere. The results confirmed that photogenerated electron–hole pairs of AgBr were effectively separated and migrated by the VB holes of AgBr transfering to the VB of $BiO(OH)_{0.06}Br_{0.94}$, and the transported holes on the VB of $BiO(OH)_{0.06}Br_{0.94}$ directly oxidized 2-CP. The pH of point of zero charge (pHpzc) values were approximately 5.0 for $BiO(OH)_{0.06}Br_{0.94}$/Ag/AgBr (Fig. 16). At the tested pH of 9, the surface of $BiO(OH)_{0.06}Br_{0.94}$/Ag/AgBr was negatively charged. Therefore, $S_2O_8^{2-}$ ions were hardly adsorbed on the sites due to electrostatic repulsion and could not trap the CB electron of AgBr, however, $S_2O_8^{2-}$ could be adsorbed on Ag NPs by complexing with photogenerated Ag^+ so that it trapped the plasmon-induced electron of Ag NPs, inhibiting the photoactivity of Ag NPs. At λ > 800 nm, the degradation of 2-CP predominantly was initiated by plasmon-induced Ag NPs. Therefore, $S_2O_8^{2-}$ ions exhibited a markedly negative effect on the 2-CP degradation (Fig. 15b), verifying that the adsorbed $S_2O_8^{2-}$ trapping plasmon-induced electron of Ag NPs. In addition, the 2-CP degradation was greatly depressed at N_2 atmosphere, indicating that the recombination rate of the plasmon-induced electrons and holes of Ag NPs was faster than that one of oxygen vacancies trapping the holes on $BiO(OH)_{0.06}Br_{0.94}$. Finally, holes and $O_2^{\bullet-}$were predominant ROS under λ > 800 nm irradiation according to the marked suppression of TEOA and *p*-benzoquinone for 2-CP degradation. Besides this, during the whole reaction, no significant Ag^+ was detected in solution. The results verified that the electrons on the oxygen vacancies of $BiO(OH)_{0.06}Br_{0.94}$ transfered to Ag NPs recombining the plasmon-induced holes, and produced holes on the VB of $BiO(OH)_{0.06}Br_{0.94}$ to oxidizing 2-CP.

On the basis of the above experimental results and band structure analysis of $BiO(OH)_{0.06}Br_{0.94}$ and AgBr, the transfer processes of charge carriers from photoexcited AgBr and Ag NPs were proposed in Fig. 17. Under visible/NIR light irradiation, in $BiO(OH)_{0.06}Br_{0.94}$/Ag/AgBr suspension, the electrons and holes

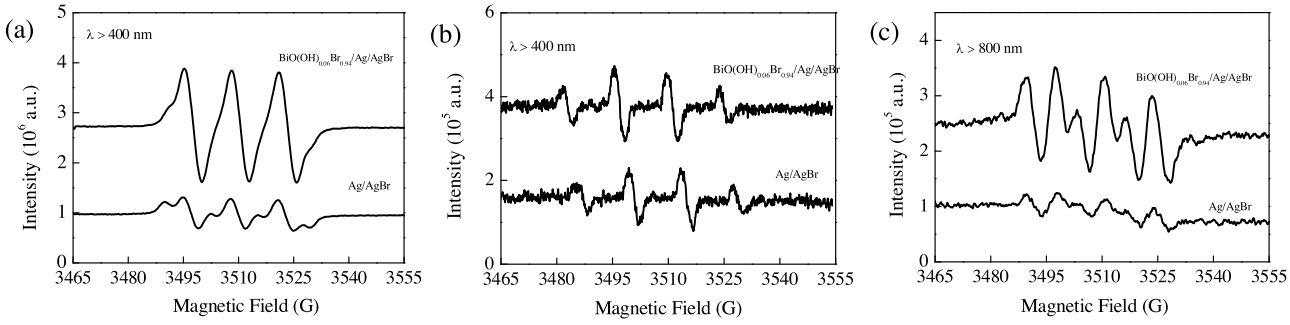

Fig. 14. BMPO spin-trapping ESR spectra in methanol dispersion for a, c) BMPO-$O_2^{\bullet-}$ and in aqueous dispersion for b) BMPO-•OH of different samples.

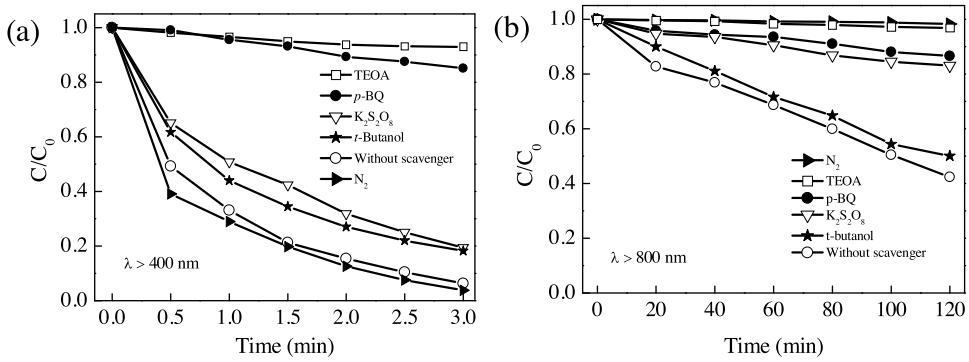

Fig. 15. Temporal course of the photodegradation of 2-CP (10 mg/L, 60 mL) in $BiO(OH)_{0.06}Br_{0.94}$/Ag/AgBr suspension (1.6 g/L) under a) visible (λ > 400 nm) or b) near infrared (λ > 800 nm) light irradiation with the addition of different radical scavengers (3 vol% TEOA, 1 mM *p*-benzoquinone, 5 mM $K_2S_2O_8$, 100 mM *t*-butanol, and N_2-bubbling systems; initial pH 9).

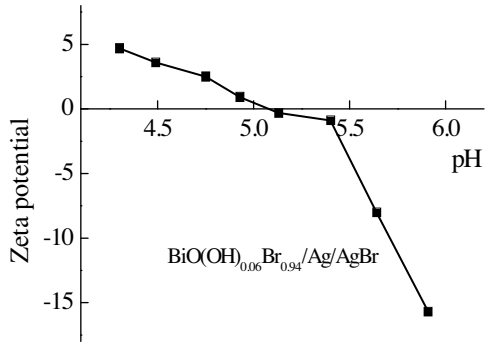

Fig. 16. Plot of the zeta potential as a function of pH for $BiO(OH)_{0.06}Br_{0.94}$/Ag/AgBr suspensions in the presence of KNO_3 (10^{-3} M).

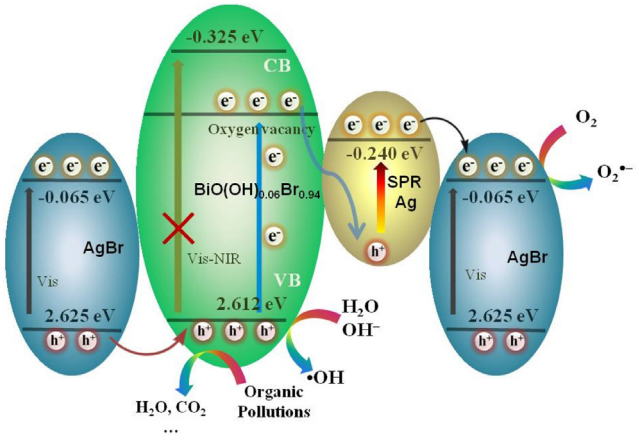

Fig. 17. The proposed transfer processes of charge carriers in photoexcited $BiO(OH)_{0.06}Br_{0.94}$/Ag/AgBr suspension.

were generated from AgBr, and the electrons transfered to the CB of AgBr to react with the adsorbed oxygen forming $O_2^{\bullet-}$, while the holes were transported the VB of $BiO(OH)_{0.06}Br_{0.94}$ to oxidiz organic pollutant or H_2O to •OH. On the other hand, the plasmon-induced electron from Ag NPs transfered to the CB of AgBr reducing the adsorbed oxygen to $O_2^{\bullet-}$, while the plasmon-induced holes on Ag NPs recombined with the electrons trapped on the oxygen vacancies of $BiO(OH)_{0.06}Br_{0.94}$, inhibiting the release of Ag^+, and the resulted VB holes of $BiO(OH)_{0.06}Br_{0.94}$ oxidized organic compound.

4. Conclusion

Solid solution of BiOBr and BHO ($BiO(OH)_{0.06}Br_{0.94}$) with abundant oxygen vacancies was supported on Ag/AgBr using precipitation and deposition–precipitation methods. The photocatalyst exhibited highly active and stable for the degradation of chlorophenols and azodyes in water under visible to NIR light irradiation without any release of Ag^+, which came from visible-excited AgBr and the SPR of Ag NPs in the visible and NIR region. Correspondingly, the CB electrons of photoexcited AgBr reacted with the adsorbed oxygen forming $O_2^{\bullet-}$, while the VB holes of AgBr were transported the VB of $BiO(OH)_{0.06}Br_{0.94}$ to oxidiz organic pollutant or H_2O to •OH. The plasmon-induced electron from Ag NPs transfered to the CB of AgBr reducing the adsorbed oxygen to $O_2^{\bullet-}$, while the electrons trapped on the oxygen vacancies of $BiO(OH)_{0.06}Br_{0.94}$ transfered to Ag NPs recombining with the plasmon-induced holes, and the resulted VB holes of $BiO(OH)_{0.06}Br_{0.94}$ oxidized organic compound. These interfacial charge transfer processes evidenced the high photoactivity and photostability of $BiO(OH)_{0.06}Br_{0.94}$/Ag/AgBr.

Acknowledgement

This work was supported by the National Natural Science Foundation of China (Grant Nos. 51538013, 21125731).

Appendix A. Supplementary data

Supplementary data associated with this article can be found, in the online version, at http://dx.doi.org/10.1016/j.apcatb.2016.06.037.

References

[1] N. Serpone, A.V. Emeline, J. Phys. Chem. Lett. 3 (2012) 673–677.
[2] R. Asahi, T. Morikawa, T. Ohwaki, K. Aoki, Y. Taga, Science 293 (2001) 269–271.
[3] S.U.M. Khan, M. Al-Shahry, W.B. Ingler Jr., Science 297 (2002) 2243–2245.
[4] Y. Sang, Z. Zhao, M. Zhao, P. Hao, Y. Leng, H. Liu, Adv. Mater. 27 (2015) 363–369.
[5] W. Fang, H. Bai, W. Shi, CrystEngComm 16 (2014) 3059–3067.
[6] Z. Zheng, T. Tachikama, T. Majima, J. Am. Chem. Soc. 136 (2014) 6870–6873.
[7] S. Linic, P. Christopher, D.B. Ingram, Nat. Mater. 10 (2011) 911–921.
[8] M. Rycenga, C.M. Cobley, J. Zeng, W. Li, C.H. Moran, Q. Zhang, D. Qin, Y. Xia, Chem. Rev. 111 (2011) 3669–3712.
[9] Y. Xia, Y. Xiong, B. Lim, S.E. Skrabalak, Angew. Chem. Int. Ed. 48 (2009) 60–103.
[10] T. Yan, X. Yan, R. Guo, W. Zhang, W. Li, J. You, Catal. Commun. 42 (2013) 30–34.
[11] L. Kong, Z. Jiang, H.H. Lai, R.J. Nicholls, T. Xiao, M.O. Jones, P.P. Edwards, J. Catal. 293 (2012) 116–125.
[12] J. Liang, J. Deng, M. Li, M. Tong, Colloids Surf. B 138 (2016) 102–109.
[13] S. Lin, L. Liu, J. Hu, Y. Liang, W. Cui, Appl. Surf. Sci. 324 (2015) 20–29.
[14] J. Li, W. Fang, C. Yu, W. Zhou, L. zhu, Y. Xie, Appl. Surf. Sci. 358 (2015) 46–56.
[15] P. Christopher, H. Xin, S. Linic, Nat. Chem. 3 (2011) 467–472.

[16] K. Awazu, M. Fujimaki, C. Rockstuhl, J. Tominaga, H. Murakami, Y. Ohki, N. Yoshida, T. Watanabe, J. Am. Chem. Soc. 130 (2008) 1676–1680.
[17] D.B. Ingram, S. Linic, J. Am. Chem. Soc. 133 (2011) 5202–5205.
[18] S. Linic, U. Aslam, C. Boerigter, M. Morabito, Nat. Mater. 14 (2015) 567–576.
[19] C.G. Silva, R. Juárez, T. Marino, R. Molinari, H. García, J. Am. Chem. Soc. 133 (2011) 595–602.
[20] C. Hu, T. Peng, X. Hu, Y. Nie, X. Zhou, J. Qu, H. He, J. Am. Chem. Soc. 132 (2010) 857–862.
[21] X. Zhou, C. Hu, X. Hu, T. Peng, J. Hazard. Mater. 219-220 (2012) 276–282.
[22] E. Kazuma, T. Tatsuma, Chem. Commun. 48 (2012) 1733–1735.
[23] S.C. Warren, E. Thimsen, Energy Environ. Sci. 5 (2012) 5133–5146.
[24] Y. Tian, T. Tatsuma, J. Am. Chem. Soc. 127 (2005) 7632–7637.
[25] V. Subramanian, E.E. Wolf, P.V. Kamat, Langmuir 19 (2003) 469–474.
[26] Y. Lv, Y. Zhu, Y. Zhu, J. Phys. Chem. C 117 (2013) 18520–18528.
[27] G. Wang, Y. Ling, Y. Li, Nanoscale 4 (2012) 6682–6691.
[28] H. Tan, Z. Zhao, W. Zhu, E.N. Coker, B. Li, M. Zheng, W. Yu, H. Fan, Z. Sun, ACS Appl. Mater. Interfaces 6 (2014) 19184–19190.
[29] A. Janotti, J.B. Varley, P. Rinke, N. Umezawa, G. Kresse, C.G. Van de Walle, Phys. Rev. B 81 (2010), 085212(7pp).
[30] X. Pan, Y.-J. Xu, Appl. Catal. A 495 (2013) 34–40.
[31] X. Pan, Y.-J. Xu, J. Phys. Chem. C 117 (2013) 17996–18005.
[32] W. Cao, O.K. Tan, J.S. Pan, W. Zhu, C.V. Gopal Reddy, Mater. Chem. Phys. 75 (2002) 67–70.
[33] K.-L. Zhang, C.-M. Liu, F.-Q. Huang, C. Zheng, W.-D. Wang, Appl. Catal. B 68 (2006) 125–129.
[34] S. Shenawi-Khalil, V. Uvarov, E. Menes, I. Popov, Y. Sasson, Appl. Catal. A 413–414 (2012) 1–9.
[35] S. Shenawi-Khalil, V. Uvarov, S. Fronton, I. Popov, Y. Sasson, J. Phys. Chem. C 116 (2012) 11004–11012.
[36] P. Wang, B. Huang, X. Zhang, X. Qin, H. Jin, Y. Dai, Z. Wang, J. Wei, J. Zhan, S. Wang, J. Wang, M.-H. Whangbo, Chem. Eur. J. 15 (2009) 1821–1824.
[37] P. Wang, B. Huang, X. Qin, X. Zhang, Y. Dai, M.-H. Whangbo, Inorg. Chem. 48 (2009) 10697–10702.
[38] C. Zhu, C. Li, M. Zheng, J.J. Delaunay, ACS Appl. Mater. Interfaces 7 (2015) 22355–22363.
[39] F. Lei, Y. Sun, K. Liu, S. Gao, L. Liang, B. Pan, Y. Xie, J. Am. Chem. Soc. 136 (2014) 6826–6829.
[40] C. Wu, L. Shen, Y.C. Zhang, Q. Huang, Mater. Lett. 66 (2012) 83–85.
[41] S. Mochizuki, J. Lumin. 70 (1996) 60–68.
[42] N.R.C. Raju, K.J. Kumar, A. Subrahmanyam, J. Phys. D: Appl. Phys. 42 (2009) 135411–135416.